Terahertz pulse induced transitions between ionic and neutral phases and electronic polarization reversal in TTF-CA

Shu Ohmura, Tomohito Mase, and Akira Takahashi

Department of Physical Science and Engineering, Nagoya Institute of Technology, Gokiso-Cho, Showa-ku, Nagoya 466-8555, Japan

We have investigated the terahertz (THz)-pulse-induced dynamics of tetrathiafulvalene-p-chloranil near the boundary between the ionic and neutral phases with the use of exact numerical calculations of an extended Hubbard model coupled with lattice motion. For the ionic phase, when the applied electric field of the THz pulse opposes the electronic contribution to the electric polarization (electronic polarization) $\bar{P}_{el}$ of the ground state and the maximum amplitude of electric field is greater than a threshold value, the THz-pulse excited state changes as $I_A \rightarrow N \rightarrow I_B \rightarrow N \rightarrow I_A \rightarrow N \rightarrow \cdots$ (I_A ground-state case) or $I_B \rightarrow N \rightarrow I_A \rightarrow N \rightarrow I_B \rightarrow N \rightarrow \cdots$ (I_B ground-state case), where N shows the neutral state, I_A (I_B) shows the ionic state with $\bar{P}_{el} < 0$ ($\bar{P}_{el} > 0$), and the phase of the bond-length alternation of I_A is opposite to that of I_B. For the neutral phase, when the maximum amplitude of the electric field is greater than a threshold value, the THz-pulse excited state changes as $N \rightarrow I_B \rightarrow N \rightarrow I_A \rightarrow N \rightarrow I_B \rightarrow \cdots$ (positive electric field case) or $N \rightarrow I_A \rightarrow N \rightarrow I_B \rightarrow N \rightarrow I_A \rightarrow \cdots$ (negative electric-field case). The phase transitions and electronic polarization reversal are driven by time variation of the lattice order parameter, which indicates the magnitude and phase of the bond-length alternation, and the lattice motion is induced by THz-pulse excitation through the electron–lattice coupling. Transitions between the ionic and neutral phases occur and electronic polarization reverses on a picosecond timescale together with the realizable magnitude of the THz pulse both in the ionic and neutral phases near the phase boundary.

I. INTRODUCTION

Recently, ferroelectricity arising from electron transfer, which is termed electronic ferroelectricity [1–3], has been observed in various materials, such as multiferroics [4–11], transition-metal oxides [12–14], and organic molecular compounds [15–34]. Ferroelectric materials are widely used in various devices, such as random access memory, capacitors, sensors, piezoelectric actuators, and optical devices [35–37]. If ferroelectric polarization could be controlled on a picosecond timescale, ferroelectric materials could be used for advanced switching devices. However, in conventional ferroelectric materials, electric polarization is governed by the rotation of polar molecules or the displacement of ions. Therefore, the typical time constants of polarization vary from micro- to milliseconds. Much faster polarization switching is expected for electronic ferroelectricity [2,3], which might open new application possibilities.

TTF-CA is an organic charge-transfer compound composed of an alternately stacked donor (D), tetrathiafulvalene (TTF), and acceptor (A), p-chloranil (CA) [38]. TTF-CA exhibits a neutral to ionic phase transition at $T_c \simeq 81$ K [38–44]. The electronic structure of these two phases is schematically shown in Fig. 1. In the ionic phase, an electron is transferred from D to A, and the phase is stable when the electrostatic energy gain overcomes the energy cost of molecular ionization. Because of orbital hybridization between D and A, the charge transfer $\bar{\rho}$ from A to D is not 1 (0), and $\bar{\rho} \sim 0.6$ ($\bar{\rho} \sim 0.3$) in the ionic (neutral) phase [45,46].

Dimerization occurs in the ionic phase [47–49]. Pairs of D and A connected by shorter bonds are indicated by the oval in Fig. 1. As a result of dimerization, inversion symmetry is broken and TTF-CA becomes ferroelectric. Previously, TTF-CA in the ionic phase had been regarded as a displacive-type ferroelectric, where polarization results from displacement of the static point charges of ions [50,51]. However, recent experimental $P - E$ measurements [15] and theoretical studies [16–19] have revealed that the direction of the net polarization is opposite to the ionic displacement and the absolute value of net polarization is much greater than that caused by ionic displacement. This result shows that the ionic phase TTF-CA is an electronic ferroelectric phase with a polarization that originates from charge transfer between D and A.

Terahertz (THz) pulses are powerful tools for investigating the ultrafast dielectric response of electronic ferroelectrics [52–55]. The THz-pump optical-probe and second-harmonic-generation-probe measurements in TTF-CA have revealed the instantaneous response of charge and the electronic contribution to the electric polarization (electronic polarization) [52]. It has been theoretically shown that the instantaneous response originates from the adiabatic nature of the THz-pulse excited state [54].

This research has focused on small changes in charge structure and electronic polarization. It has been experimentally shown that in the paraelectric neutral phase, the magnitude of polarization is increased to about 20% of that in the ferroelectric ionic phase by intense THz-pulse excitation, and the large increase is attributed to breathing motions of domain walls between neutral and ionic domains induced by the THz electric field [56]. However, ultrafast polarization reversal, which is required for applications in advanced devices, in
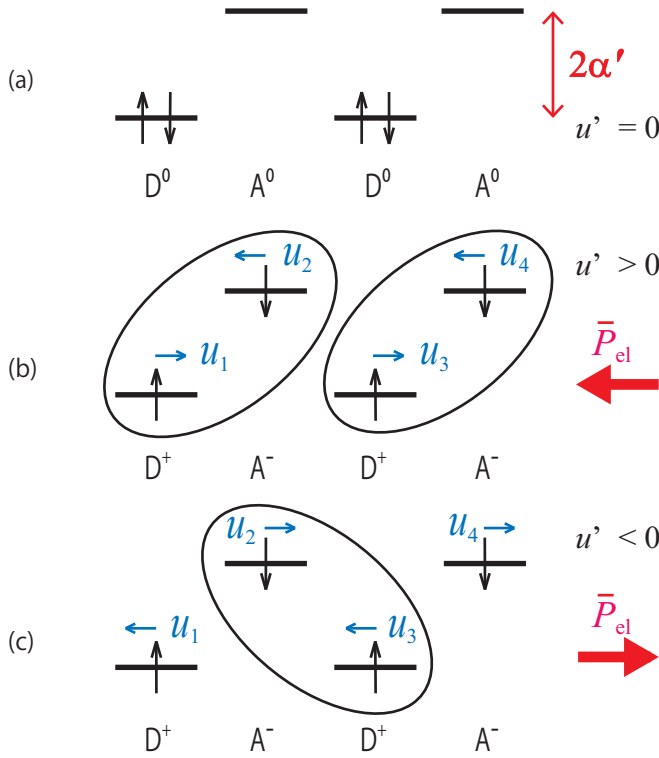
FIG. 1. Schematic representation of the electronic structures of (a) neutral phase (N), (b) ionic phases with A phase bond-length alternation (I$_A$), and (c) ionic phases with B phase bond-length alternation (I$_B$) of TTF-CA. Horizontal lines show the highest occupied molecular orbital of D and the lowest unoccupied molecular orbital of A, and arrows represent the electron spins. Neutral (ionic) D and A are denoted by D^0 and A^0 (D$^+$ and A$^-$), respectively.

the ionic phase has not been observed in these experimental and theoretical investigations [52,54,56]. Furthermore, if the phase transition is induced by THz-pulse excitation, which is far-off resonance to the optical gap, the mechanism is essentially different from that of a photo-induced phase transition between the neutral and ionic phases [57–67], which is triggered by real excitation. There has been a rapid development of correlated systems far from equilibrium that are driven by strong alternating current electric fields [68–74]. THz-pulse-induced phase transitions are a key example of this interesting phenomena.

In a previous investigation, it has been shown that charge susceptibility is markedly enhanced near the phase boundary [54]. Furthermore, THz-pulse excitation may induce lattice motion, which reverses the phase of bond-length alternation and the electronic polarization. In this paper, we therefore investigate the THz-pulse-induced dynamics near the phase boundary, accounting for the effects of electron-lattice coupling, to investigate the possibility of polarization reversal and THz-pulse-induced phase transitions.

II. MODEL

We adopt the extended Hubbard Hamiltonian for TTF-CA, which includes coupling with lattice motion and with the electric field of a THz pulse. We consider a half-filled periodic

1D chain with system size $N = 14$. The Hamiltonian at time t is given by

$$
H(t) = \sum_{n=1}^{N} (-1)^n \alpha' n_n + \sum_{n=1,\sigma}^{N} \{\beta_n(t) c_{n,\sigma}^{\dagger} c_{n+1,\sigma} + \text{H.c.}\}
$$
$$
+ U \sum_{n=1}^{N} n_{n,\uparrow} n_{n,\downarrow} + V \sum_{n=1}^{N} n_n n_{n+1}
$$
$$
+ \frac{1}{2} K \sum_{n=1}^{N} \{u_{n+1}(t) - u_n(t)\}^2 + \frac{1}{2} M \sum_{n=1}^{N} \left(\frac{du_n(t)}{dt} \right)^2,
$$
(1)

where D (A) is placed at odd–numbered (even–numbered) sites. The first term describes the site energy, where $2\alpha'$ shows the difference in orbital energy between the highest occupied molecular orbital of D and the lowest unoccupied molecular orbital of A (see Fig. 1), $n_n = \sum_\sigma n_{n,\sigma}$, $n_{n,\sigma} = c_{n,\sigma}^{\dagger} c_{n,\sigma}$, and $c_{n,\sigma}^{\dagger}$ ($c_{n,\sigma}$) creates (annihilates) an electron of spin σ at site n. The second term describes the transfer of electrons, and the electron–lattice coupling and electron–field coupling are introduced into the transfer integrals. The transfer integral between sites n and $n + 1$ at time t is given by

$$
\beta_n(t) = \{\bar{\beta} + u_{n+1}(t) - u_n(t)\} \exp[ieaA(t)],
$$
(2)

where $\bar{\beta}$ is the transfer integral for the uniform lattice, $u_n(t)$ is the displacement along the chain direction from the position of uniform lattice at site n, $A(t)$ is the one-dimensional component of vector potential, $a = 3.6$ Å is the average lattice spacing along the one-dimensional direction, and e is the elementary charge. We take account of the dependence of β_n on $u_{n+1}(t)$ and $u_n(t)$ only to the first order, and the unit of $u_n(t)$ is adopted so the absolute value of the differential coefficient is 1. The third and the fourth terms describe the on-site Coulomb interaction and the Coulomb interaction between neighboring sites, respectively, where U is the on-site Coulomb interaction energy and V is the Coulomb interaction energy between neighboring sites. The fifth term describes the bond deformation energy, where K is the elastic coefficient, and the sixth term shows the kinetic energy of lattice motion, where M is the mass of each molecule. We assume that the masses of D and A molecules are the same for simplicity.

The THz-pulse-excited electron-lattice state is obtained by numerically solving the time-dependent Schrödinger equation and classical equation of motion for lattice subject to the Hellmann–Feynman force simultaneously. The time-dependent Schrödinger equation,

$$
i \frac{\partial}{\partial t} |\psi(t)\rangle = H(t) |\psi(t)\rangle,
$$
(3)

is solved by employing the time-dependent exact diagonalization method with the initial condition $|\psi(-\infty)\rangle = |\phi_0\rangle$, where $|\psi(t)\rangle$ is the electronic state at time t and the ground state $|\phi_0\rangle$ is obtained by the the Lanczos method. The classical equation of motion for lattice is given by

$$
M \frac{d^2}{dt^2} u_n(t) = F_n(t),
$$
(4)

where $F_n(t)$ is the Hellmann–Feynman force acting on site n, and is given by

$$F_n(t) = [\langle \psi(t)| \sum_\sigma (c_{n,\sigma}^\dagger c_{n+1,\sigma} - c_{n-1,\sigma}^\dagger c_{n,\sigma})|\psi(t)\rangle$$
$$\times \exp[ieaA(t)] + \text{H.c.}] + K[u_{n+1}(t)$$
$$+ u_{n-1}(t) - 2u_n(t)]. \tag{5}$$

Because of the translational symmetry, $u_n(t)$ satisfies the relation

$$u_n(t) = (-1)^{n-1} u'(t). \tag{6}$$

The lattice order parameter (LOP) $u'(t)$ is defined by the alternating component $u_n(t)$, and the lattice state is given by this single quantity. The absolute value and the sign of $u'(t)$ represent the magnitude and the phase of the bond-length alternation, respectively. We impose the initial condition $u'(-\infty) = u_0'$, where u_0' is the LOP of the ground state.

The ground state $|\phi_0\rangle$ of the present model is calculated as follows. We consider the adiabatic Hamiltonian given by

$$H_{\text{AP}}(u') = \sum_{n=1}^N (-1)^n \alpha' n_n + \sum_{n=1,\sigma}^N \{\bar{\beta} + 2(-1)^n u'\}\{c_{n,\sigma}^\dagger c_{n+1,\sigma}$$
$$+ \text{H.c.}\} + U \sum_{n=1}^N n_{n,\uparrow} n_{n,\downarrow} + V \sum_{n=1}^N n_n n_{n+1}$$
$$+ 2NK(u')^2, \tag{7}$$

where the electron–field coupling is not considered and the lattice displacements are fixed to that given by the LOP u'. The electron and lattice structures are determined consistently so the force equilibrium condition $F_{\text{AP}}(u') = -\frac{\partial}{\partial u'} E_0(u') = 0$ is satisfied, where $E_0(u')$ is the energy eigenvalue for the ground state $|\phi_0(u')\rangle$ of $H_{\text{AP}}(u')$. From the Hellmann–Feynman theory, $F_{\text{AP}}(u')$ is given by

$$F_{\text{AP}}(u') = 4 \sum_{n=1,\sigma}^N (-1)^{n-1} \langle \phi_0(u')|c_{n,\sigma}^\dagger c_{n+1,\sigma}|\phi_0(u')\rangle - 4NKu'. \tag{8}$$

Because of the inversion symmetry, the force equilibrium is always satisfied at $u' = 0$. Furthermore, if the force equilibrium is satisfied at $u' = u_{\text{eq}}' > 0$, then force equilibrium is also satisfied at $u' = -u_{\text{eq}}'$, and $E_0(u_{\text{eq}}') = E_0(-u_{\text{eq}}')$ holds. If $E(0) < E(u_{\text{eq}}')$ holds, the ground state $|\phi_0\rangle$ is given by $|\phi_0(0)\rangle$ and the LOP for the ground state is given by $u_0' = 0$. If $E(0) > E(u_{\text{eq}}')$ holds, the ground state is twofold degenerate, and $|\phi_0\rangle = |\phi_0(\pm u_{\text{eq}}')\rangle$ and $u_0' = \pm u_{\text{eq}}'$ hold.

III. RESULTS

It has been shown that the light absorption spectrum $\alpha_0(\omega)$ of the neutral phase, where $u_0' = 0$ holds, can be reproduced well with the following parameters: $\bar{\beta} = -0.17$, $\alpha' = 0.15$, $U = 2.41$, and $V = 1.07$ [57]. Here and hereafter, we use eV as the unit of energy. The above values of $\bar{\beta}$, U, and V are adopted for both the neutral and ionic phases. The parameter α' is used to control the distance from the phase boundary. We mainly consider the THz-pulse-induced dynamics at the
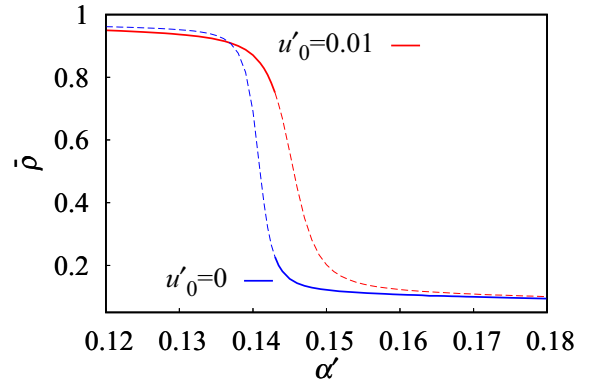

FIG. 2. The α' dependence of $\bar{\rho}$ for the ground and metastable states are shown by solid and dashed lines, respectively.

phase boundary between the ionic and neutral phases, and adopt $\alpha' = 0.143$ at which these two phases are degenerate in energy, as will be discussed later. In the ionic phase, bond-length alternation occurs ($u_0' \neq 0$ holds), and $\alpha_0(\omega)$ depends on K through u_0'. The light absorption spectrum $\alpha_0(\omega)$ of the ionic phase can be reproduced reasonably around $|u_0'| = 0.01$ in the realistic region of α' with these adopted $\bar{\beta}$, U, and V. The value is consistent with the length difference between the longer and shorter bonds [47]. Therefore, K is determined from Eq. (8) so $|u_0'| = 0.01$ holds. The mass M is determined so that the bare phonon frequency $2\sqrt{K/M}$ is equal to that of the THz-pulse-induced coherent oscillation of $\Delta R/R$ (6.70 × 10^{-3}), which is associated with the dimerization mode [52]. These parameters are consistent with previous theoretical works [16,44,75–79].

Because of the translational symmetry, the charge distribution of the ground state is given by the single quantity $\bar{\rho}$, which is the charge transfer from A to D for the ground state, and given by

$$\bar{\rho} = \langle \phi_0|n_2|\phi_0\rangle. \tag{9}$$

In the ionic (neutral) phase $\bar{\rho} \simeq 1$ ($\bar{\rho} \simeq 0$) holds. As shown before, between the two electron lattice states $|\phi_0(0)\rangle$ with $u' = 0$ and $|\phi_0(\pm u_{\text{eq}}')\rangle$ with $u' = \pm u_{\text{eq}}'$, one is the ground state and the other is a metastable state. We calculated the ground state and the metastable state for various α' with the interval of 0.0005, and show the α' dependence of $\bar{\rho}$ for these two states in Fig. 2. Note that different K is adopted for different α' to give $u_{\text{eq}}' = 0.01$. The relation $E(0) = E(u_{\text{eq}}')$ holds at $\alpha' = 0.143$. For $\alpha' < 0.143$ ($\alpha' > 0.143$), $|\phi_0(\pm u_{\text{eq}}')\rangle$ with $u' = \pm u_{\text{eq}}'$ ($|\phi_0(0)\rangle$ with $u' = 0$) is the ground state and $\bar{\rho} \simeq 1$ ($\bar{\rho} \simeq 0$) holds, showing that the ground state is ionic (neutral). We mainly consider the THz-pulse-induced dynamics at the phase boundary (at $\alpha' = 0.143$, where $K = 17.496$ gives $|u_0'| = 0.01$) in the following. The characteristic features shown below are commonly observed near the phase boundary, as will be discussed later.

The ground states are twofold degenerate in the ionic phase, and they have the same amplitude but opposite phases of bond-length alternation as shown in Figs. 1(b) and 1(c). These two degenerate ionic phases are denoted by A and B, and $u_0' > 0$ ($u_0' < 0$) holds and the odd–numbered bonds are
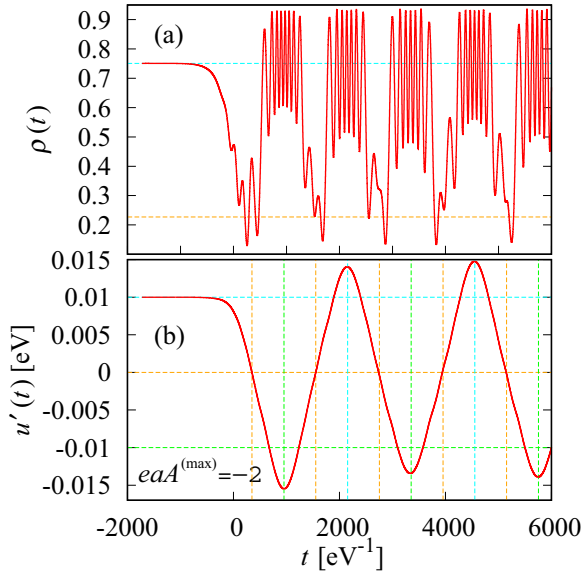
FIG. 3. Temporal profiles of (a) $\rho(t)$ and (b) $u'(t)$ are shown by solid lines when the A phase ionic ground state is excited by the half-cycle pulse with $eaA^{(\mathrm{max})} = -2$. Horizontal dashed lines in (a) show the charge transfer $\bar{\rho} = 0.751$ for the ionic ground state and $\bar{\rho} = 0.227$ for the neutral ground state at the phase boundary. Horizontal dashed lines in (b) show the LOP $u'_0 = \pm 0.01$ for the ionic ground state and $u'_0 = 0$ for the neutral ground state, and vertical dashed lines in (b) indicate the times when $u'(t) = 0$ holds and those when $u'(t)$ exhibits local maxima or local minima.
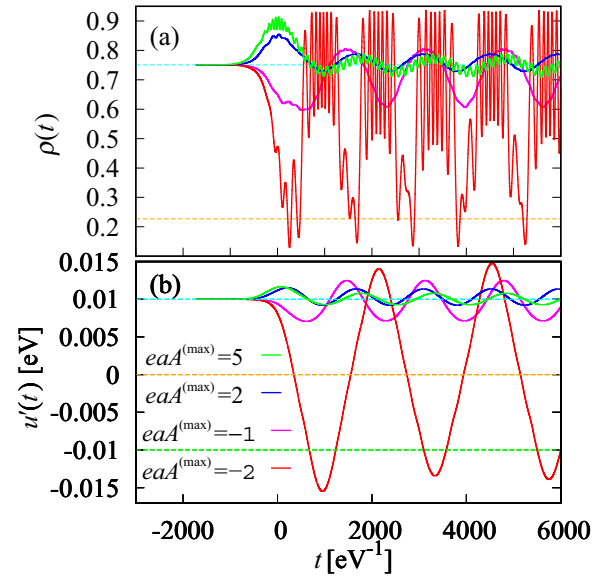

FIG. 4. Temporal profiles of (a) $\rho(t)$ and (b) $u'(t)$ are shown by the solid lines when the A phase ionic ground state is excited by the half-cycle pulse with $eaA^{(\mathrm{max})} = -2, -1, 2,$ and 5. Horizontal dashed lines in (a) show the charge transfer $\bar{\rho} = 0.751$ for the ionic ground state and $\bar{\rho} = 0.227$ for the neutral ground state at the phase boundary. Horizontal dashed lines in (b) show the LOP $u'_0 = \pm 0.01$ for the ionic ground state and $u'_0 = 0$ for the neutral ground state.

shorter (longer) than even-numbered bonds in phase A (B), where bond n connects sites n and $n + 1$. Directly calculating the adiabatic flow of current of the many-body wave function has shown that $\bar{P}_{\mathrm{el}} < 0$ ($\bar{P}_{\mathrm{el}} > 0$) holds for the A (B) phase ionic ground state, where $\bar{P}_{\mathrm{el}}$ is the electronic polarization and $\bar{P}_{\mathrm{el}} > 0$ ($\bar{P}_{\mathrm{el}} < 0$) shows that $\bar{P}_{\mathrm{el}}$ points in the direction of increasing (decreasing) site number [54]. The polarization direction is consistent with experimental results [15] and previous theoretical calculations based on density-functional theory [16–19].

We first consider the electron and lattice dynamics in the ionic phase induced by the THz pulse given by the vector potential of a half-cycle pulse:

$$A(t) = \frac{A^{(\mathrm{max})}}{2}\left\{1 + \tanh\left(\frac{t}{D}\right)\right\}, \quad (10)$$

where $A^{(\mathrm{max})}$ is the maximum amplitude and D is the pulse duration. The electric field of the pulse is given by

$$E(t) = -\frac{1}{2eaD}eaA^{(\mathrm{max})}\cosh^{-2}\left(\frac{t}{D}\right), \quad (11)$$

where $E(t) > 0$ ($E(t) < 0$) holds when the electric field points in the direction of increasing (decreasing) site number. We adopt the duration time $D = 300$ eV^{-1} (201 fs), which is approximately the same as that used in the experiments [52,53] and $1/(2eaD) = 46$ kV/cm. We adopt the A phase ionic ground state as an initial state. For $A^{(\mathrm{max})} > 0$ ($A^{(\mathrm{max})} < 0$), the electric field is in the same (opposite) direction of the electronic polarization of the ground state. The charge transfer $\rho(t)$ for the THz-pulse excited state $|\psi(t)\rangle$ is

given by

$$\rho(t) = \langle\psi(t)|n_2|\psi(t)\rangle. \quad (12)$$

We show the temporal profiles of $\rho(t)$ and $u'(t)$ when the I$_A$ ground state is excited by the THz pulse with $eaA^{(\mathrm{max})} = -2$, where I$_A$ (I$_B$) shows the A (B) phase ionic state, in Fig. 3. In this strong excitation case when the electric field of the THz-pulse is applied opposite to the electronic polarization, $u'(t)$ exhibits a large amplitude oscillation. The center of the oscillation is located near zero, and the local maximum values of $|u'(t)|$ are greater than $|u'_0| = 0.01$. The charge transfer $\rho(t)$ has slowly and rapidly oscillating components, and the amplitude of the former is much greater than that of the latter. Around times when $u'(t) = 0$, $\rho(t)$ is close to $\bar{\rho} = 0.227$ for the neutral ground state at the phase boundary, and around times when $|u'(t)|$ exhibits local maximum values, $\rho(t)$ is close to $\bar{\rho} = 0.751$ for the ionic ground state at the phase boundary. Therefore, the THz-pulse excited state changes as I$_A \to$ N $\to$ I$_B \to$ N $\to$ I$_A \to$ N $\to \cdots$, where N shows the neutral state without bond-length alternation, and the phase transition between ionic and neutral phases occurs.

We show $\rho(t)$ and $u'(t)$ for various $eaA^{(\mathrm{max})}$ in Fig. 4. The charge transfer $\rho(t)$ and the magnitude of bond-length alternation $|u'(t)|$ initially increase (decrease) when the electric field of the THz-pulse is applied in the direction (opposite direction) of the electronic polarization. This result can be understood from the balance of the currents between the odd-numbered and the even-numbered bonds. From the equation of charge conservation, time variation of charge transfer is given by the difference between the time integrations of the

current at the odd-numbered and even-numbered bonds as

$$\rho(t_2) - \rho(t_1) = \frac{1}{e}[\{I_2(t_2) - I_2(t_1)\} - \{I_1(t_2) - I_1(t_1)\}], \quad (13)$$

where

$$I_n(t_2) - I_n(t_1) = \int_{t_1}^{t_2} dt\, i_n(t), \quad (14)$$

is the time integration of the expectation value $i_n(t) = \langle\psi(t)|\hat{i}_n(t)|\psi(t)\rangle$ of the current operator $\hat{i}_n$ for bond n given by

$$\hat{i}_n(t) = -ie\sum_\sigma\{\beta_n(t)c_{n,\sigma}^\dagger c_{n+1,\sigma} - \text{H.c.}\}. \quad (15)$$

In the initial I_A state with $\bar{P}_{el} < 0$, $|\beta_1(t)|$ is considerably greater than $|\beta_2(t)|$ as a result of A-phase bond-length alternation [see Eq. (2) and Fig. 1(b)]. When $E(t) < 0$ ($E(t) > 0$), namely, the electric field is applied to the same (opposite) direction of the electronic polarization, the time integrations of $i_n(t)$ are negative (positive). Whereas, $|i_1(t)|$ is considerably greater than $|i_2(t)|$, as a result of the considerable difference in $|\beta_n(t)|$ between odd-numbered and even-numbered bonds [see Eq. (15)] in both cases, which results in the initial increase (decrease) in $\rho(t)$ when the electric field is applied in the same (opposite) direction of the electronic polarization.

As $\rho(t)$ approaches 1, the bond orders $p_n(t) = \text{Re}[\langle\psi(t)|\sum_\sigma c_{n,\sigma}^\dagger c_{n+1,\sigma}|\psi(t)\rangle]$ for shorter bonds increase. Therefore, the initial increase (decrease) in $\rho(t)$ induces the initial increase (decrease) in $|u'(t)|$ as shown by the Hellmann–Feynman force given in Eq. (8). The D and A molecules gain momentum as a result of initial lattice motion, and the oscillation of $u'(t)$ continues after the pulse has gone off. This result contrasts with the instantaneous charge response characteristics of the fixed lattice case.

For $eaA^{(\text{max})} = -1$, the center of the oscillation in $u'(t)$ is located near $u'_0 = 0.01$ and the sign of $u'(t)$ is not reversed. The amplitude of the oscillation in $\rho(t)$ is much smaller than that for $eaA^{(\text{max})} = -2$, and $\rho(t)$ is constantly much greater than $\bar{\rho} = 0.227$ for the neutral ground state at the phase boundary. Thus, the phase transition does not occur for $eaA^{(\text{max})} = -1$. The phase transition occurs when $|eaA^{(\text{max})}|$ is greater than a threshold value in the case when the electric field of the applied THz pulse opposes the electronic polarization.

Next, we consider the case when the electric field of the THz-pulse is applied in the direction of the electronic polarization. For $eaA^{(\text{max})} = 2$ and 5, both $u'(t)$ and $\rho(t)$ exhibit small amplitude oscillations, and the phase transition does not occur in the realistic $eaA^{(\text{max})}$ region in this case.

We have calculated the THz-pulse-induced dynamics of charge transfer $\rho^{(\text{fix})}(t)$, when the lattice is fixed to that of the ground state, to consider the effects of lattice motion. In this case, the THz-pulse induced change $\rho^{(\text{fix})}(t) - \bar{\rho}$ in the charge transfer is negligibly small after the pulse has gone off in all the considered cases. This result also shows that the phase transitions and also the continuing oscillation after the pulse are both induced by lattice motion. This holds also in the THz-pulse-induced dynamics of the neutral ground-state case.

Finally, we consider the electronic polarization per unit cell $P_{el}(t)$ of the THz-pulse excited state $|\psi(t)\rangle$. We emphasize that $P_{el}(t)$ cannot be determined from the charge distribution in the unit cell of $|\psi(t)\rangle$, but can be determined from the current flow [80–83]. The current can be calculated from the Berry phase in models based on density-functional theory [80,84] and other methods have been proposed [85,86]. In this paper, we directly calculate the current from the many-body wave function to fully take the strong correlation effect into account. The electronic polarization variation induced by the THz pulse is given by the time integration of current flow as

$$P_{el}(t) - P_{el}(t_0) = a[\{I_2(t) - I_2(t_0)\} + \{I_1(t) - I_1(t_0)\}]. \quad (16)$$

As shown in our previous paper, $i_n(t)$ is strongly affected by this finite-size effect when $A(t) \neq 0$ [54,55]. We therefore consider the dynamics induced by the double half-cycle pulses. The vector potential of the double pulses is given by

$$A(t) = \frac{A^{(\text{max})}}{2}\left\{\tanh\left(\frac{t}{D}\right) - \tanh\left(\frac{t - t_d}{D}\right)\right\}, \quad (17)$$

where t_d is the delay of the second pulse. In the case of the double pulses, $A(t)$ is effectively zero and therefore a finite-size effect is negligible in calculating $P_{el}(t)$ by Eq. (16) in the time region $t \gg t_d + D$.

We show the temporal profiles of $\rho(t)$, $P_{el}(t) - P_{el}(t_0)$, $I_n(t) - I_n(t_0)$, and $u'(t)$ for $eaA^{(\text{max})} = -2$ in Fig. 5 in the time region where $A(t)$ is effectively zero. We adopt the delay $t_d = 1900$ so the second pulse interferes constructively with the lattice motion induced by the first pulse. We see that the phase transition between ionic and neutral phases also occurs in the double pulse case.

We have calculated the overlap $\langle\phi_0(u'(t))|\psi(t)\rangle$ between the THz-pulse excited state $|\psi(t)\rangle$ and the ground state $|\phi_0(u'(t))\rangle$ of the adiabatic Hamiltonian with the LOP $u'(t)$. We consider the time region where $A(t)$ is effectively zero in the double-pulse excitation case to exclude the finite-size effect arising from constant and nonzero vector potential. The absolute value $|\langle\phi_0(u'(t))|\psi(t)\rangle|$ is about 0.98 in the time region, and this large overlap shows that $|\psi(t)\rangle$ changes nearly adiabatically with the time variation of $u'(t)$. Therefore, the phase transitions between the ionic and neutral phases are induced by the cooperative lattice motion, and the barrier height in the adiabatic potential connecting the $\text{I}_A - \text{N} - \text{I}_B$ states is the determining factor of the threshold for the phase transition.

The time $t_0 = 4693.6$ is chosen so $u'(t_0) = 0$ holds. Because of the adiabatic nature, $|\psi(t_0)\rangle$ is approximately given by the neutral ground state and $P_{el}(t_0) \simeq 0$ holds. The electronic polarization $P_{el}(t)$ around times when $u'(t)$ exhibits local maxima and those around times when $u'(t)$ exhibits local minima have almost the same magnitudes but the opposite signs. The polarization reversal occurs as a result of the lattice motion induced by THz-pulse excitation.

Furthermore, the proportional relation $-\text{sgn}[u'(t)][\rho(t) - \rho(t_0)] = [P_{el}(t) - P_{el}(t_0)]/(ea)$ holds quite nicely. Because of the adiabatic nature, $|\psi(t)\rangle$ becomes very close to the neutral ground state at the times t_0, $t_1 = 5738.4$, $t_2 = 6780.7$, and $t_3 = 7822.9$, where $u'(t_i) = 0$ holds, and $I_1(t_{i+1}) - I_1(t_i) \simeq 0$ and $I_2(t_{i+1}) - I_2(t_i) \simeq 0$ hold. In the time
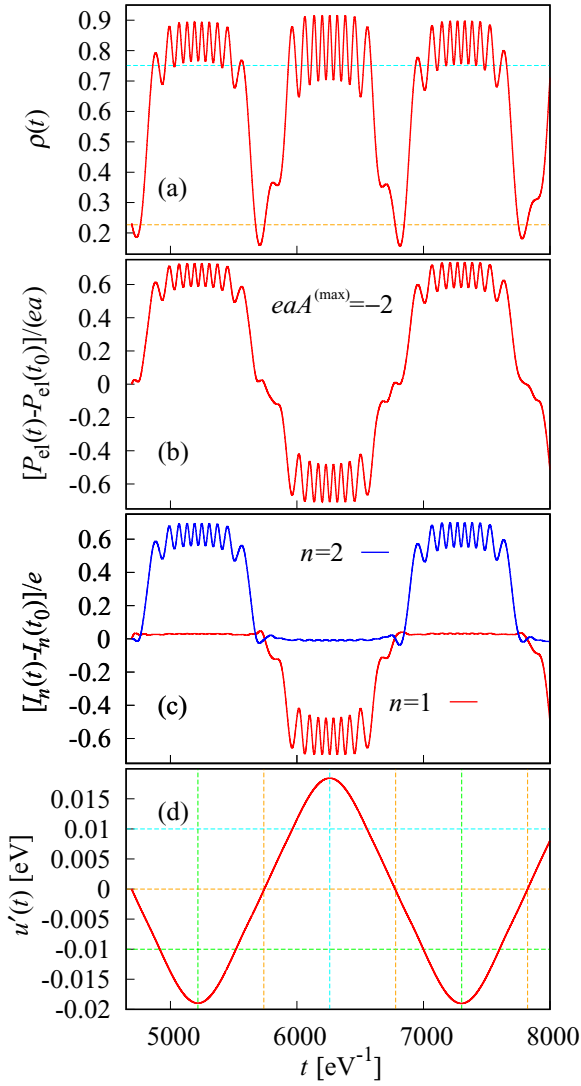
FIG. 5. Temporal profiles of (a) $\rho(t)$, (b) $P_{el}(t) - P_{el}(t_0)$, (c) $I_1(t) - I_1(t_0)$ and $I_2(t) - I_2(t_0)$ with $t_0 = 4693.6$, and (d) $u'(t)$ are shown by the solid lines when the A phase ionic ground state is excited by the double half-cycle pulses with $eaA^{(max)} = -2$ and $t_d = 1900$. Horizontal dashed lines in (a) show the charge transfer $\bar{\rho} = 0.751$ for the ionic ground state and $\bar{\rho} = 0.227$ for the neutral ground state at the phase boundary. Horizontal dashed lines in (d) show the LOP $u'_0 = \pm 0.01$ for the ionic ground state and $u'_0 = 0$ for the neutral ground state, and vertical dashed lines in (d) indicate times when $u'(t) = 0$ holds and those when $u'(t)$ exhibits local maxima or local minima.

region $t_i < t < t_{i+1}$ where $|\psi(t)\rangle$ changes as N → I$_A$ → N (N → I$_B$ → N), $u'(t) > 0$ [$u'(t) < 0$] and therefore $|\beta_1(t)| > |\beta_2(t)|$ ($|\beta_1(t)| < |\beta_2(t)|$) hold. Charge transfer through bonds with larger $|\beta_n(t)|$ is dominant, and $|I_1(t) - I_1(t_i)| \gg |I_2(t) - I_2(t_i)|$ ($|I_1(t) - I_1(t_i)| \ll |I_2(t) - I_2(t_i)|$) hold in most of the time region as seen from Fig. 5(c). The proportional relation can be derived from this relation. It is noted that the charge transfer of stronger bonds is predominant even in the time region where the difference between the larger one and the smaller one is only about 10%, and the proportional relation comes from this property. This result is consistent with
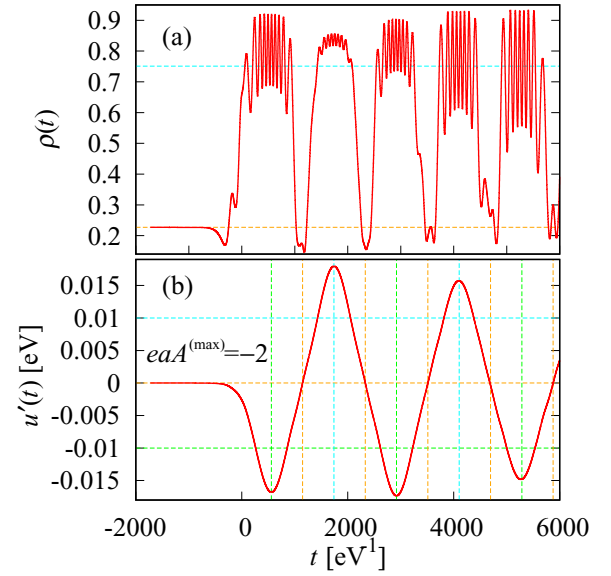

FIG. 6. Temporal profiles of (a) $\rho(t)$ and (b) $u'(t)$ are shown by the solid lines when the neutral ground state is excited by the half-cycle pulses with $eaA^{(max)} = -2$. Horizontal dashed lines in (a) show the charge transfer $\bar{\rho} = 0.751$ for the ionic ground state and $\bar{\rho} = 0.227$ for the neutral ground state at the phase boundary. Horizontal dashed lines in (b) show the LOP $u'_0 = \pm 0.01$ for the ionic ground state and $u'_0 = 0$ for the neutral ground state, and vertical dashed lines in (b) indicate the times when $u'(t) = 0$ holds and those when $u'(t)$ exhibits local maxima or local minima.

the THz-pulse-induced charge transfer in α-(BEDT-TTH)$_2$I$_3$ [55]. Note that $I_1(t) - I_1(t_i) < 0$ and $I_2(t) - I_2(t_i) > 0$ in the dominant time region because acceptor molecules are placed at even-numbered sites.

We next consider the electron and lattice dynamics in the neutral phase induced by the THz pulse given by the vector potential of a half-cycle pulse. We show the temporal profiles of $\rho(t)$ and $u'(t)$ induced by the half-cycle pulse given by Eq. (10) for $eaA^{(max)} = -2$ in Fig. 6. In this strong excitation case, $\rho(t)$ and $u'(t)$ exhibit large amplitude oscillations. From the same discussion as the ionic phase, we see that the THz-pulse excited state changes as N → I$_B$ → N → I$_A$ → N → I$_B$ → ⋯. The phase transition between ionic and neutral phases occurs also in this case. The phase transition due to breathing motions of domain walls between neutral and ionic domains [56] is not considered in the present investigation in the spatially uniform system.

We show $\rho(t)$ and $u'(t)$ for various $eaA^{(max)}$ in Fig. 7. The charge transfer $\rho(t)$ for $A^{(max)} = A_0$, where A_0 is a constant, coincides with $\rho(t)$ for $A^{(max)} = -A_0$, and $u'(t)$ for $A^{(max)} = A_0$ coincides with $-u'(t)$ for $A^{(max)} = -A_0$. For $|eaA^{(max)}| = 0.5$, the amplitudes of the oscillations in $\rho(t)$ and $u'(t)$ are much smaller than those for $|eaA^{(max)}| \geqslant 1$, and $\rho(t)$ ($|u'(t)|$) is constantly much smaller than the charge transfer $\bar{\rho} = 0.751$ (the magnitude of LOP $|u'_0| = 0.01$) for the ionic ground state at the phase boundary. This result shows that the phase transition occurs when $|eaA^{(max)}|$ is greater than a threshold value. The phase transition and polarization reversal occur both for $eaA^{(max)} \lesssim -1$ and for $eaA^{(max)} \gtrsim 1$ in this case. The LOP $u'(t)$ initially increases (decreases) for

FIG. 8. $|W_\rho(t,\omega)|$ for $eaA^{(\max)} = -2$ for the neutral ground state
at the phase boundary. The frequency $\omega_p(u')$ of the lowest in-gap
peak versus time t that satisfies the relation $u'(t) = u'$ is shown by
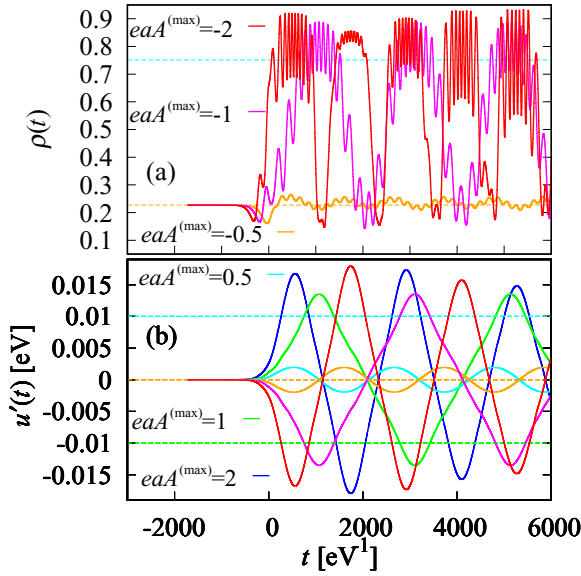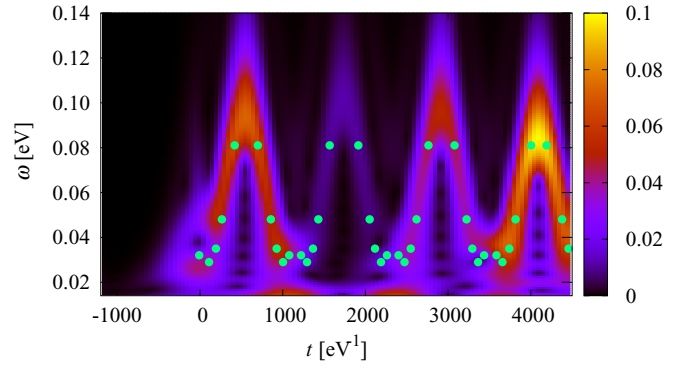dots at $u' = \pm 0.00250, \pm 0.005, \pm 0.0075, \pm 0.01$, and ± 0.015.

FIG. 7. Temporal profiles of (a) $\rho(t)$ and (b) $u'(t)$ are shown by
solid lines when the neutral ground state is excited by the half-cycle
pulses with $eaA^{(\max)} = -2, -1, -0.5, 0.5, 1$, and 2. Horizontal
dashed lines in (a) show the charge transfer $\bar\rho = 0.751$ for the ionic
ground state and $\bar\rho = 0.227$ for the neutral ground state at the phase
boundary. Horizontal dashed lines in (b) show the LOP $u'_0 = \pm 0.01$
for the ionic ground state and $u'_0 = 0$ for the neutral ground state.

$eaA^{(\max)} > 0$ ($eaA^{(\max)} < 0$). As a result, the I$_A$ (I$_B$) phase
with negative (positive) $P_{el}(t)$ is initially generated when the
electric field of the THz pulse is negative (positive).

We next consider the rapidly oscillating component of $\rho(t)$
seen in Figs. 3–7. We perform a wavelet transformation of
$\rho(t)$ given by

$$W_\rho(t,\omega) = \frac{1}{s}\int_{-\infty}^{\infty}\rho(\tau)w\left(\frac{\tau - t}{s}\right)d\tau, \qquad (18)$$

where s is the scale parameter and $w(x)$ is a mother wavelet.
In the present study, we chose the Morlet wavelet

$$w(x) = \exp(i\omega_0 x)\exp\left(-\frac{x^2}{2}\right), \qquad (19)$$

where ω_0 is the dimensionless frequency and we set $\omega_0 = 6.0$.
Then, the frequency ω corresponding to s is given by $\omega =
2\pi/(1.05s)$ [87].

We show $|W_\rho(t,\omega)|$ for $A^{(\max)} = -2$ in the case of neutral
ground state in Fig. 8. The peak frequency $\omega_{\max}(t)$, where
$|W_\rho(t,\omega)|$ is greatest at $\omega = \omega_{\max}(t)$ for a given t, changes
with time, and $\omega_{\max}(t)$ in the time region of the ionic phase is
considerably greater than that in the time regions of the phase
transitions.

To understand the origin of the oscillation, we show
in Fig. 9 the absorption spectrum $\alpha_0(\omega)$ for the ground
state $|\phi_0(u')\rangle$ of the adiabatic Hamiltonian $H_{AP}(u')$ at $\alpha' =
0.143$ for a given LOP u'. Small peaks exist inside the gap
($\Delta E \simeq 0.5$) in $\alpha_0(\omega)$. The frequency $\omega_p(u')$ of the lowest
in-gap peak depends on u', and we also plot $\omega_p(u')$ versus
time t that satisfies the relation $u'(t) = u'$ in Fig. 8. The peak
frequency $\omega_p(u')$ agrees well with $\omega_{\max}(t)$. This result comes
from adiabatic nature of $|\psi(t)\rangle$. As shown in the Appendix,

$|\psi(t)\rangle$ is given by the linear combination of energy eigenstates
of $H_{AP}(u'(t))$, and the coefficient $c_n(t)$ of the excited stated is
given by Eq. (A9) if the adiabatic approximation holds well. In
the considered time region, $E(t)$ is effectively zero, and $c_n(t)$
is proportional to $\{du'(t)/dt\}\omega_n^{-2}(t)$. This shows that energy
eigenstates of $H_{AP}(u'(t))$ are excited by the lattice motion.
Furthermore, since the excitation energies $\omega_n(t)$ of the in-gap
states are about $1/10$ of ΔE, the in-gap states have dominant
weights among the excited states, and the excitation of an
in-gap state induces the oscillation of $\rho(t)$ with the frequency
of the excitation energy of the state. This is the origin of the
rapidly oscillating term in $\rho(t)$. The adiabatic behavior can
be attributed to the fact that the period of $u'(t)$ oscillation is
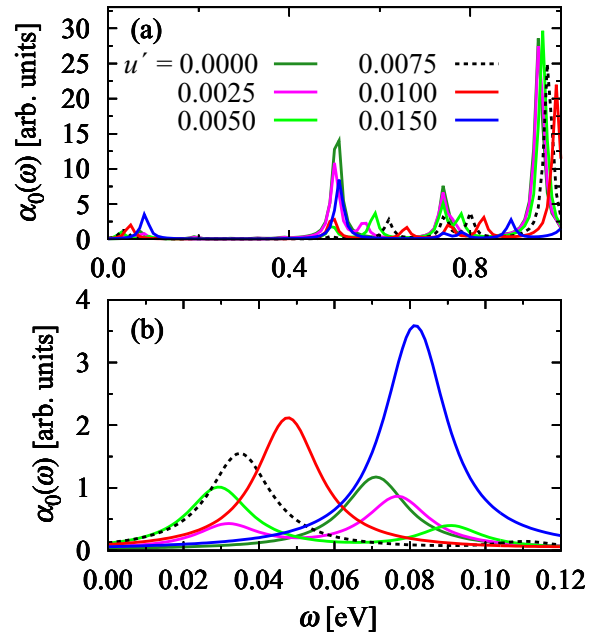approximately ten times as long as the inverse of the lowest

FIG. 9. (a) Absorption spectrum $\alpha_0(\omega)$ and (b) $\alpha_0(\omega)$ in the
in-gap region for the ground state $|\phi_0(u')\rangle$ of the adiabatic Hamil-
tonian $H_{AP}(u')$ for $u' = 0, 0.0025, 0.005, 0.0075, 0.01$, and 0.015 at
$\alpha' = 0.143$.

in-gap peak energy, which ensures that $\epsilon_2 \ll 1$ holds, where ϵ_2 is a small parameter of the adiabatic approximation given in Eq. (A11), and the adiabatic approximation is valid.

We have discussed the THz-pulse-induced dynamics at the phase boundary. To investigate how the dynamics depends on the distance from the phase boundary, we have calculated the dynamics with various α' at $eaA^{(\mathrm{max})} = -2$. The THz-pulse-induced phase transition occurs in the range $0.1425 \leqslant \alpha' \leqslant 0.146$ near the phase boundary. The amplitudes of oscillations in $\rho(t)$ and $u'(t)$ decrease rapidly as α' is decreased from 0.1425 and as α' is increased from 0.146. As shown in Fig. 2, the difference between the charge transfer for the ground state and that for the metastable state is much smaller than 1 for $\alpha' \lesssim 0.13$ and for $\alpha' \gtrsim 0.16$. In the α' region, the instantaneous change dominates in $\rho(t)$, and $\rho(t)$ is almost the same as that in the case of a fixed lattice. The effect of lattice motion is negligible, and large changes of the electronic state induced by lattice motion do not occur in this region.

From numerical calculations, it is shown that the period of the oscillation of $u'(t)$ depends not only on the distance from the phase boundary α' but also on the amplitude $A^{(\mathrm{max})}$ of the THz pulse. This can be understood as follows. The lattice motion can be approximately described as the dynamics on the adiabatic potential. We numerically calculated the adiabatic potential and confirmed that the potential strongly depends on α'. In the phase boundary region, there are three local minimums corresponding to I_A, N, and I_B states. The LOP $u'(t)$ changes between the three local minimums crossing two potential barriers when the lattice structure changes as $I_A \rightarrow N \rightarrow I_B$. The motion is quite anharmonic and, therefore, the period depends also on the injected energy by the THz pulse excitation, which depends on $A^{(\mathrm{max})}$.

IV. SUMMARY AND DISCUSSIONS

We have investigated the THz-pulse induced dynamics of TTF-CA near the phase boundary using exact numerical calculations of an extended Hubbard model coupled with lattice motion. For the ionic phase, when the applied electric field of the THz-pulse opposes the electronic polarization of the ground state and the maximum amplitude of the electric field is greater than a threshold value, which is in realizable region, the THz-pulse excited state changes as $I_A \rightarrow N \rightarrow I_B \rightarrow N \rightarrow I_A \rightarrow N \rightarrow \cdots$ (I_A ground-state case) or $I_B \rightarrow N \rightarrow I_A \rightarrow N \rightarrow I_B \rightarrow N \rightarrow \cdots$ (I_B ground-state case). When the applied electric field opposes the electronic polarization and the maximum amplitude of the electric field is smaller than the threshold value, and when the field of the applied THz pulse is in the direction of the electronic polarization, neither the phase transition nor polarization reversal occurs. For the neutral phase, when the maximum amplitude of the electric field is greater than a threshold value, the THz-pulse excited state changes as $N \rightarrow I_B \rightarrow N \rightarrow I_A \rightarrow N \rightarrow I_B \rightarrow \cdots$ ($E(t) > 0$ case) or $N \rightarrow I_A \rightarrow N \rightarrow I_B \rightarrow N \rightarrow I_A \rightarrow \cdots$ ($E(t) < 0$ case). The LOP, which shows the magnitude and phase of bond-length alternation, is considerably changed by THz-pulse excitation through electron-lattice coupling, and

the phase transitions and polarization reversal are driven by lattice motion in these strongly excited cases.

We have succeeded in showing that the phase transitions between ionic phases with different phases of bond-length alternation and a neutral phase occur and electronic polarization reverses on a picosecond timescale with a realizable magnitude of the THz pulse both in the ionic and neutral phases near the phase boundary. However, in the present results, the electronic polarization oscillates with time and control of electronic polarization is not realized. The threshold behavior shows that there exists an energy barrier between the ionic and neutral phases. As a result of the injection energy required to exceed the energy barrier, $|u'(t)|$ becomes greater than $|u'_0| = 0.01$ for the ionic ground state at the local maxima, and this overshoot results in the oscillation of $u'(t)$. Therefore, there is a possibility that a stable targeted final state can be realized by applying a second THz pulse that disturbs the lattice motion after the excited state generated by the first pulse has passed over the energy barrier. We will consider designing a pulse shape that can control the final state in our future study.

There is a possibility that the phase transition is induced by dielectric breakdown. We have confirmed that the phase transition shown in this paper is not due to the dielectric breakdown from the following numerical results. First, we roughly estimate the threshold E_{db} of direct current electric filed for dielectric breakdown. As shown in previous paper, the threshold is roughly given by $E_{\mathrm{db}} = \Delta E/(2ea\xi)$, where ξ is the correlation length [88]. Adopting the maximum distance in the periodic chain as the correlation length ($\xi = N/2$), and $\Delta E = 0.5$ eV, we estimate the amplitude $A_{\mathrm{db}}^{(\mathrm{max})}$ of the vector potential that gives E_{db} as $ea|A_{\mathrm{db}}^{(\mathrm{max})}| = 2eaDE_{\mathrm{db}} \sim 20$. The estimated value is much larger than the threshold amplitude $ea|A^{(\mathrm{max})}| \sim 1$ of the phase transition. Second, if the phase transition is induced by the dielectric breakdown, then the maximum electric field $E^{(\mathrm{max})} = A^{(\mathrm{max})}/(2D)$ is the factor determining whether the phase transition occurs or not. We have compared the THz-pulse-induced dynamics in the case of neutral ground state for the following three parameter sets: $(eaA^{(\mathrm{max})}, D) = (1, 300)$, $(1/2, 150)$, and $(1/3, 100)$, which give the same $E^{(\mathrm{max})}$. The phase transition occurs only for $(eaA^{(\mathrm{max})}, D) = (1, 300)$, and does not occur in the other cases, showing that $E^{(\mathrm{max})}$ is not the factor. Third, we have numerically calculated the adiabatic potential as a function of LOP u' at various α'. The adiabatic potential drastically changes but the optical gap ΔE and therefore E_{db} change slightly as α' is changed from the value $\alpha' = 0.143$ at the phase boundary. The THz-pulse-induced phase transition occurs only in the phase boundary region $0.1425 \leqslant \alpha' \leqslant 0.146$, which is inconsistent with the phase transition due to dielectric breakdown.

We have calculated the THz-pulse-induced dynamics up to the amplitudes nearly equal to the estimated $A_{\mathrm{db}}^{(\mathrm{max})}$. The phase transitions occur for $eaA^{(\mathrm{max})} = -20$, where the applied electric field opposes the electronic polarization of the ground state, even outside the phase boundary region. Outside the phase boundary region, the THz-pulse-induced variation of the charge transfer $\rho(t)$ is very small, and the phase transition between ionic and neutral phases does not

occur within the realizable amplitude $ea|A^{(\text{max})}| \lesssim 10$. The variation increases rapidly with increasing $|A^{(\text{max})}|$ around $|A^{(\text{max})}| = |A_{\text{db}}^{(\text{max})}|$ and the THz-pulse-induced phase transition occurs for $|A^{(\text{max})}| \gtrsim |A_{\text{db}}^{(\text{max})}|$ both in the case of ionic ground state when the electric field of the applied THz-pulse opposes the electronic polarization and in the case of the neutral ground state. The characteristic $A^{(\text{max})}$ dependence of the dynamics suggests that the phase transition arises from dielectric breakdown. This conclusion is also consistent with the fact that the phase transition occurs outside the phase boundary region. Furthermore, we have numerically confirmed that purely electronic transition phase transition is induced by the THz pulse for $|A^{(\text{max})}| \gtrsim |A_{\text{db}}^{(\text{max})}|$ when the lattice is fixed to that of the ground state. The electronic origin of the transition is also consistent with the conclusion. The phase transitions does not occur around $|A^{(\text{max})}| = |A_{\text{db}}^{(\text{max})}|$ when the electric field of the THz pulse is applied in the direction of the electronic polarization of the ionic ground state. In this case, an acceptor orbital with higher energy level becomes doubly occupied as a result of the dielectric breakdown and the energy cost for the dielectric breakdown is much larger than ΔE.

Recently, a paraelectric ionic phase with a uniform lattice has been found in the high-pressure and high-temperature region [89,90], and it has been proposed that bond-length alternation is destroyed by thermal or quantum fluctuations of soliton pairs in the phase, where a soliton is a topological defect between I_A and I_B domains [89–92]. If a thermally excited confined pair of oppositely charged solitons exists in the I_A phase, then a I_B domain exists between the solitons. Because solitons are movable, the I_B domain can be increased by translational motion of solitons, and the electronic polarization may be reversed as a result of the charged soliton motion induced by the electric field of the THz pulse. In the present paper, we investigated the dynamics when a translationally symmetric ground state is excited by the spatially uniform electric field of the THz pulse at zero temperature. The above-mentioned mechanism of polarization reversal is not considered. Numerical calculations of dynamics at finite temperatures are a difficult problem, but we might investigate this mechanism by analyzing the THz-pulse-induced dynamics from the initial states with charged solitons. Polarization reversal may arise from quantum fluctuations of charged soliton pairs. However, the present system size $N = 14$ is too small to include soliton pairs as quantum fluctuations. To investigate these mechanisms for polarization reversal, we need to establish an effective model where the THz-pulse-induced dynamics can be calculated taking the effects of soliton pairs into account in large systems.

APPENDIX

In this Appendix, we derive the condition under which the adiabatic approximation holds well by extending the results obtained in Ref. [54] to the electron–lattice coupled case. Up to the first order of the small parameters ϵ_1 and ϵ_2 of the adiabatic approximation, which will be described later, the solution $|\psi(t)\rangle$ of the time-dependent Schrödinger equation can be written as

$$|\psi(t)\rangle = \exp\left[-i\int_0^t d\tau E_0(\tau)\right]|\phi_0(t)\rangle + |\delta\psi(t)\rangle, \quad (A1)$$

$$|\delta\psi(t)\rangle = \sum_n^{n\neq 0} c_n(t) \exp\left[-i\int_0^t d\tau E_n(\tau)\right]|\phi_n(t)\rangle, \quad (A2)$$

where $|\phi_n(t)\rangle$ is the energy eigenstate of $H(t)$ with an energy eigenvalue $E_n(t)$, and $|\phi_0(t)\rangle$ and $E_0(t)$ are the ground state and the ground-state energy, respectively. Note that the magnitude of the coefficient for $|\phi_0(t)\rangle$ is equal to 1 up to the first order. The first-order term $|\delta\psi(t)\rangle$ is given by the linear combination of $|\phi_n(t)\rangle$ with the coefficient $c_n(t)$.

To derive differential equation for $c_n(t)$, we consider the terms up to the first order of infinitesimal time change Δt in the following. We divide the Hamiltonian $H(t + \Delta t)$ into the unperturbed part $H_0(t) = H(t)$ and perturbed part $H_1(t) = H(t + \Delta t) - H(t)$. Up to the first order of Δt, $H_1(t)$ can be written as

$$H_1 = \hat{J}(t)eaE(t)\Delta t + \hat{K}(t)\frac{du'(t)}{dt}\Delta t, \quad (A3)$$

where $\hat{J}(t)$ is given by

$$\hat{J}(t) = \frac{1}{e}\sum_{n=1}^N \hat{i}_n, \quad (A4)$$

and $\hat{K}(t)$ is given by

$$\hat{K}(t) = 2\sum_{n=1,\sigma}^N (-1)^n \{c_{n,\sigma}^\dagger c_{n+1,\sigma}\exp[ieaA(t)] + \text{H.c.}\}. \quad (A5)$$

Here we neglect the term describing the bond deformation energy because it gives the same phase factor for all the coefficients $c_n(t)$.

As shown in Ref. [54], from the time-dependent perturbation theory, it can be shown that $c_n(t)$ satisfies the following differential equation:

$$\frac{d}{dt}c_n(t) = \exp\left[i\int_0^t d\tau\omega_n(\tau)\right]\left\{\frac{J_{n,0}(t)}{\omega_n(t)}eaE(t)\right. \\ \left. + \frac{K_{n,0}(t)}{\omega_n(t)}\frac{du'(t)}{dt}\right\}, \quad (A6)$$

where $J_{n,k}(t)$ is the transition dipole moment given by

$$J_{n,k}(t) = \langle\phi_n(t)|\hat{J}|\phi_k(t)\rangle, \quad (A7)$$

$$K_{n,k}(t) = \langle\phi_n(t)|\hat{K}|\phi_k(t)\rangle, \quad (A8)$$

and $\omega_n(t) = E_n(t) - E_0(t)$ is the excitation energy from the ground state to the energy eigenstate $|\phi_n(t)\rangle$.

The coefficients $c_n(t)$ are given by time integration of the right-hand side of Eq. (A6), and repeating integration by parts of on the time integration, we obtain a series expansion of $c_n(t)$ in terms of small parameters $1/(\omega_n D)$ and $1/(\omega_n T)$. Here T is the timescale of lattice motion, and $d^n u'(t)/dt^n$ is the order of $(1/T)^n$. Considering the off-resonant case and

neglecting the terms of second order or more in $1/(\omega_n D)$ and $1/(\omega_n T)$, we obtain

$$c_n(t) = -i \exp\left[i \int_0^t d\tau \, \omega_n(\tau)\right] \left\{\frac{J_{n,0}(t)}{\omega_n^2(t)} eaE(t)\right.$$
$$\left. + \frac{K_{n,0}(t)}{\omega_n^2(t)} \frac{du'(t)}{dt}\right\}. \quad \text{(A9)}$$

In the case of THz pulse excitation, $1/(\Delta ED) \ll 1$ holds for almost all the insulators. If the lattice motion is slow enough to satisfy $1/(\Delta ET) \ll 1$, this approximation holds well.

Therefore, the small parameters for the adiabatic approximation are given by

$$\epsilon_1 = \max\left(\frac{|J_{n,0}|}{\omega_n^2}\right)\frac{ea|A^{(\max)}|}{D}, \quad \text{(A10)}$$

$$\epsilon_2 = \max\left(\frac{|K_{n,0}|}{\omega_n^2}\right)\left|\frac{du'}{dt}\right|, \quad \text{(A11)}$$

and the adiabatic approximation is good if $\epsilon_1 \ll 1$ and $\epsilon_2 \ll 1$ hold.

---

[1] T. Portengen, Th. Östreich, and L. J. Sham, Phys. Rev. B **54**, 17452 (1996).

[2] J. van den Brink and D. I. Khomskii, J. Phys. Condens. Matter **20**, 434217 (2008).

[3] S. Ishihara, J. Phys. Soc. Jpn. **79**, 011010 (2010).

[4] T. Kimura, T. Goto, H. Shintani, K. Ishizaka, T. Arima, and Y. Tokura, Nature (London) **426**, 55 (2003).

[5] J. Wang, J. B. Neaton, H. Zheng, V. Nagarajan, S. B. Ogale, B. Liu, D. Viehland, V. Vaithyanathan, D. G. Schlom, U. V. Waghmare, N. A. Spaldin, K. M. Rabe, M. Wuttig, and R. Ramesh, Science **299**, 1719 (2003).

[6] N. A. Spaldin and M. Fiebig, Science **309**, 391 (2005).

[7] W. Eerenstein, N. D. Mathur, and J. F. Scott, Nature (London) **442**, 759 (2006).

[8] S.-W Cheong and M. Mostovoy, Nat. Mater. **6**, 13 (2007).

[9] S. Picozzi, K. Yamauchi, B. Sanyal, I. A. Sergienko, and E. Dagotto, Phys. Rev. Lett. **99**, 227201 (2007).

[10] D. Khomskii, Physics **2**, 20 (2009).

[11] P. Lunkenheimer, J. Müller, S. Krohns, F. Schrettle, A. Loidl, B. Hartmann, R. Rommel, M. de Souza, C. Hotta, J. A. Schlueter, and M. Lang, Nat. Mater. **11**, 755 (2012).

[12] N. Ikeda, H. Ohsumi, K. Ohwada, K. Ishii, T. Inami, K. Kakurai, Y. Murakami, K. Yoshii, S. Mori, Y. Horibe, and H. Kito, Nature (London) **436**, 1136 (2005).

[13] A. Nagano, M. Naka, J. Nasu, and S. Ishihara, Phys. Rev. Lett. **99**, 217202 (2007).

[14] M. Naka, A. Nagano, and S. Ishihara, Phys. Rev. B **77**, 224441 (2008).

[15] K. Kobayashi, S. Horiuchi, R. Kumai, F. Kagawa, Y. Murakami, and Y. Tokura, Phys. Rev. Lett. **108**, 237601 (2012).

[16] G. Giovannetti, S. Kumar, A. Stroppa, J. van den Brink, and S. Picozzi, Phys. Rev. Lett. **103**, 266401 (2009).

[17] S. Ishibashi and K. Terakura, Phys. B (Amsterdam) **405**, S338 (2010).

[18] S. Ishibashi and K. Terakura, J. Phys. Soc. Jpn. **83**, 073702 (2014).

[19] K. Terakura and S. Ishibashi, Phys. Rev. B **91**, 195120 (2015).

[20] P. Monceau, F. Ya. Nad, and S. Brazovskii, Phys. Rev. Lett. **86**, 4080 (2001).

[21] H. Yoshioka, M. Tsuchiizu, and H. Seo, J. Phys. Soc. Jpn. **76**, 103701 (2007).

[22] Y. Otsuka, H. Seo, Y. Motome, and T. Kato, J. Phys. Soc. Jpn. **77**, 113705 (2008).

[23] K. Yamamoto, S. Iwai, S. Boyko, A. Kashiwazaki, F. Hiramatsu, C. Okabe, N. Nishi, and K. Yakushi, J. Phys. Soc. Jpn. **77**, 074709 (2008).

[24] K. Yamamoto, A. Kowalska, and K. Yakushi, Appl. Phys. Lett. **96**, 122901 (2010).

[25] P. Lunkenheimer, B. Hartmann, M. Lang, J. Müller, D. Schweitzer, S. Krohns, and A. Loidl, Phys. Rev. B **91**, 245132 (2015).

[26] M. Abdel-Jawad, I. Terasaki, T. Sasaki, N. Yoneyama, N. Kobayashi, Y. Uesu, and C. Hotta, Phys. Rev. B **82**, 125119 (2010).

[27] H. Gomi, T. Imai, A. Takahashi, and M. Aihara, Phys. Rev. B **82**, 035101 (2010).

[28] M. Naka and S. Ishihara, J. Phys. Soc. Jpn. **79**, 063707 (2010).

[29] C. Hotta, Phys. Rev. B **82**, 241104(R) (2010).

[30] S. Dayal, R. T. Clay, H. Li, and S. Mazumdar, Phys. Rev. B **83**, 245106 (2011).

[31] K. Itoh, H. Itoh, M. Naka, S. Saito, I. Hosako, N. Yoneyama, S. Ishihara, T. Sasaki, and S. Iwai, Phys. Rev. Lett. **110**, 106401 (2013).

[32] M. Naka and S. Ishihara, J. Phys. Soc. Jpn. **82**, 023701 (2013).

[33] H. Gomi, M. Ikenaga, Y. Hiragi, D. Segawa, A. Takahashi, T. J. Inagaki, and M. Aihara, Phys. Rev. B **87**, 195126 (2013).

[34] H. Gomi, T. J. Inagaki, and A. Takahashi, Phys. Rev. B **93**, 035105 (2016).

[35] K. Uchino, *Ferroelectric Devices* (Marcel Dekker, New York, 2000).

[36] M. E. Lines and A. M. Glass, *Principles and Applications of Ferroelectrics and Related Materials* (Oxford University, New York, 1977).

[37] J. F. Scott, Science **315**, 954 (2007).

[38] J. B. Torrance, J. E. Vazquez, J. J. Mayerle, and V. Y. Lee, Phys. Rev. Lett. **46**, 253 (1981).

[39] H. M. McConnell, B. M. Hoffman, and R. M. Metzger, Proc. Natl. Acad. Sci. USA **53**, 46 (1965).

[40] J. B. Torrance, A. Girlando, J. J. Mayerle, J. I. Crowley, V. Y. Lee, P. Batail, and S. J. LaPlaca, Phys. Rev. Lett. **47**, 1747 (1981).

[41] M. H. Lemée-Cailleau, M. Le Cointe, H. Cailleau, T. Luty, F. Moussa, J. Roos, D. Brinkmann, B. Toudic, C. Ayache, and N. Karl, Rev. Lett. **79**, 1690 (1997)

[42] A. Girlando, A. Painelli, S. Bewick, and Z. Soos, Synth. Met. **141**, 129 (2004).

[43] M. Masino, A. Girlando, A. Brillante, R. G. Della Valle, E. Venuti, N. Drichko, and M. Dressel, Chem. Phys. **325**, 71 (2006)

[44] G. D'Avino and M. J. Verstraete, Phys. Rev. Lett. **113**, 237602 (2014)

[45] A. Girlando, F. Marzola, C. Pecile, and J. B. Torrance, J. Chem. Phys. **79**, 1075 (1983).

[46] S. Horiuchi, Y. Okimoto, R. Kumai, and Y. Tokura, J. Phys. Soc. Jpn. **69**, 1302 (2000).

[47] M. Le Cointe, M. H. Lemee-Cailleau, H. Cailleau, B. Toudic, L. Toupet, G. Heger, F. Moussa, P. Schweiss, K. H. Kraft, and N. Karl, Phys. Rev. B **51**, 3374 (1995).

[48] Y. Tokura, S. Koshihara, Y. Iwasa, H. Okamoto, T. Komatsu, T. Koda, N. Iwasawa, and G. Saito, Phys. Rev. Lett. **63**, 2405 (1989).

[49] P. Garcia, S. Dahaoui, C. Katan, M. Souhassou, and C. Lecomte, Faraday Discuss. **135**, 217 (2007).

[50] H. Okamoto, T. Mitani, Y. Tokura, S. Koshihara, T. Komatsu, Y. Iwasa, T. Koda, and G. Saito, Phys. Rev. B **43**, 8224 (1991).

[51] H. Kishida, H. Takamatsu, K. Fujinuma, and H. Okamoto, Phys. Rev. B **80**, 205201 (2009).

[52] T. Miyamoto, H. Yada, H. Yamakawa, and H. Okamoto, Nat. Commun. **4**, 2586 (2013).

[53] H. Yamakawa, T. Miyamoto, T. Morimoto, H. Yada, Y. Kinoshita, M. Sotome, N. Kida, K. Yamamoto, K. Iwano, Y. Matsumoto, S. Watanabe, Y. Shimoi, M. Suda, H. M. Yamamoto, H. Mori, and H. Okamoto, Sci. Rep. **6**, 20571 (2016).

[54] H. Gomi, N. Yamagishi, T. Mase, T. J. Inagaki, and A. Takahashi, Phys. Rev. B **95**, 094116 (2017).

[55] S. Kuniki, S. Ohmura, and A. Takahashi, Phys. Rev. B **98**, 165149 (2018).

[56] T. Morimoto, T. Miyamoto, H. Yamakawa, T. Terashige, T. Ono, N. Kida, and H. Okamoto, Phys. Rev. Lett. **118**, 107602 (2017).

[57] K. Iwano, Phys. Rev. Lett. **97**, 226404 (2006).

[58] K. Yonemitsu, J. Phys. Soc. Jpn. **80**, 084707 (2011).

[59] T. Luty, H. Cailleau, S. Koshihara, E. Collet, M. Takesada, M. H. Lemee-Cailleau, M. Buron-Le Cointe, N. Nagaosa, Y. Tokura, E. Zienkiewicz, and B. Ouladdiaf, Europhys. Lett. **59**, 619 (2002).

[60] E. Collet, M.-H. Leme-Cailleau, M. Buron-Le Cointe, H. Cailleau, M. Wulff, T. Luty, S.-Y. Koshihara, M. Meyer, L. Toupet, P. Rabiller, and S. Techert, Science **300**, 612 (2003).

[61] H. Okamoto, Y. Ishige, S. Tanaka, H. Kishida, S. Iwai, and Y. Tokura, Phys. Rev. B **70**, 165202 (2004).

[62] H. Uemura and H. Okamoto, Phys. Rev. Lett. **105**, 258302 (2010).

[63] T. Miyamoto, K. Kimura, T. Hamamoto, H. Uemura, H. Yada, H. Matsuzaki, S. Horiuchi, and H. Okamoto, Phys. Rev. Lett. **111**, 187801 (2013).

[64] K. Iwano, Phys. Rev. Lett. **102**, 106405 (2009).

[65] K. Iwano, Phys. Rev. B **84**, 235139 (2011).

[66] Y. Nakatsuka, T. Tsuneda, T. Sato, and K. Hirao, J. Chem. Theory Comput. **7**, 2233 (2011).

[67] L. Cavatorta, A. Painelli, and Z. G. Soos, Phys. Rev. B **91**, 174301 (2015).

[68] N. Tsuji, T. Oka, P. Werner, and H. Aoki, Phys. Rev. Lett. **106**, 236401 (2011).

[69] N. Tsuji, T. Oka, H. Aoki, and P. Werner, Phys. Rev. B **85**, 155124 (2012).

[70] K. Yonemitsu and K. Nishioka, J. Phys. Soc. Jpn. **84**, 054702 (2015).

[71] H. Yanagiya, Y. Tanaka, and K. Yonemitsu, J. Phys. Soc. Jpn. **84**, 094705 (2015).

[72] A. Ono, H. Hashimoto, and S. Ishihara, Phys. Rev. B **94**, 115152 (2016).

[73] A. Ono, H. Hashimoto, and S. Ishihara, Phys. Rev. B **95**, 085123 (2017).

[74] K. Oya and A. Takahashi, Phys. Rev. B **97**, 115147 (2018).

[75] N. Nagaosa and J. Takimoto, J. Phys. Soc. Jpn. **55**, 2735 (1986).

[76] A. Painelli and A. Girlando, Phys. Rev. B **37**, 5748 (1988).

[77] L. Del Freo, A. Painelli, and Z. G. Soos, Phys. Rev. Lett. **89**, 027402 (2002).

[78] M. Tsuchiizu and A. Furusaki, Phys. Rev. B **69**, 035103 (2004).

[79] Z. G. Soos, S. A. Bewick, A. Peri, and A. Painelli, J. Chem. Phys. **120**, 6712 (2004).

[80] R. D. King-Smith and D. Vanderbilt, Phys. Rev. B **47**, 1651 (1993).

[81] R. Resta, Rev. Mod. Phys. **66**, 899 (1994).

[82] R. E. Cohen, Nature (London) **358**, 136 (1992).

[83] T. Egami, S. Ishihara, and M. Tachiki, Science **261**, 1307 (1993).

[84] D. Vanderbilt and R. D. King-Smith, Phys. Rev. B **48**, 4442 (1993).

[85] S. Onoda, S. Murakami, and N. Nagaosa, Phys. Rev. Lett. **93**, 167602 (2004).

[86] R. Nourafkan and G. Kotliar, Phys. Rev. B **88**, 155121 (2013).

[87] S. D. Meyers, B. G. Kelly, and J. J. O'brien, Mon. Wea. Rev. **121**, 2858 (1993).

[88] T. Oka, Phys. Rev. B **86**, 075148 (2012)

[89] R. Takehara, K. Sunami, F. Iwase, M. Hosoda, K. Miyagawa, T. Miyamoto, H. Okamoto, and K. Kanoda, Phys. Rev. B **98**, 054103 (2018)

[90] K. Sunami, T. Nishikawa, K. Miyagawa, S. Horiuchi, R. Kato, T. Miyamoto, H. Okamoto, and K. Kanoda, Sci. Adv. **4**, 7725 (2018).

[91] H. Fukuyama and M. Ogata, J. Phys. Soc. Jpn. **85**, 023702 (2016).

[92] M. Tsuchiizu, H. Yoshioka, and H. Seo, J. Phys. Soc. Jpn. **85**, 104705 (2016).